The Influence of Strain Rate on the Mode III Interlaminar Fracture of Composite Materials

D. Pennas, W.J. Cantwell and P. Compston

Journal of Composite Materials 2007; 41; 2595
DOI: 10.1177/0021998307078690

The Influence of Strain Rate on the Mode III Interlaminar Fracture of Composite Materials

D. PENNAS AND W. J. CANTWELL*
Department of Engineering, University of Liverpool
Liverpool L69 3GH, UK

P. COMPSTON
Department of Engineering, FEIT, Australian National University
Canberra ACT200, Australia

ABSTRACT: The Mode III interlaminar fracture toughness, G_{IIIc}, of composite materials based on both thermoplastic and thermosetting-matrices have been investigated using the edge crack torsion (ECT) test geometry. Tests were undertaken at room temperature and over a range of crosshead displacement rates to study the influence of strain rate on the interlaminar fracture properties of these materials. Further information concerning the crack tip loading conditions was obtained by undertaking a finite element analysis of the ECT specimen geometry.

The experimental results show that the value of G_{IIIc} depends on initial crack length, increasing steadily with increasing crack length for both types of material. It has been shown that the interlaminar fracture toughness of the glass fiber/epoxy-based system was superior to that offered by its thermoplastic counterpart, an effect that may be due to the fact that the glass fiber-reinforced polypropylene composite was slow-cooled from its processing temperature. The interlaminar fracture toughness of both types of composite remained roughly constant over the range of crosshead displacement rates considered here suggesting that they do not exhibit any rate-sensitive fracture behavior. The finite element analysis of the ECT specimens showed that the specimen is subjected to pure Mode III loading over the central part of the test specimen whereas regions of locally-high Mode II loading were observed over the region in which the load was applied. The Mode III strain energy release rate profile does not depend on specimen thickness or the displacement of the ECT test geometry.

KEY WORDS: interlaminar fracture, delamination, carbon fiber epoxy, impact.

*Author to whom correspondence should be addressed. E-mail: w.cantwell@loverpool.ac.uk
Figures 2 and 3 appear in color online: http://jcm.sagepub.com

0021-9983/07/21 2595–20 $10.00/0 DOI: 10.1177/0021998307078690

Los Angeles, London, New Delhi and Singapore

INTRODUCTION

COMPOSITE MATERIALS BASED on strong, stiff fibers in a polymeric matrix are currently finding increasing use in a range of primary load-bearing aerospace structures. Composites offer a number of key advantages over more conventional monolithic materials including high specific strength and stiffness, excellent corrosion resistance as well as a superior formability. One of the most cited disadvantages of these composite materials is their poor resistance to localized impact loading. Previous work has shown that low energy impacts are capable of generating significant damage within a composite structure that can, in turn, result in a significant reduction in its load-carrying capability [1–5]. Detailed examinations of the fractured composite components have identified a number of fracture mechanisms such as delamination, fiber fracture and matrix cracking. Of these, delamination is perhaps the most serious since it can significantly reduce the compressive strength of the composite component [1].

In an attempt to characterize the delamination resistance of high performance composite materials, researchers have used a variety of test techniques such as the double cantilever beam (DCB), the end-notch flexure (ENF), and the split cantilever beam (SCB) [6–11]. Much of this work has been undertaken at relatively low strain rates, far removed from those encountered under impact conditions. It is, however, well known that many of the polymeric materials used in the manufacture of composite materials are rate-sensitive with their fracture toughness properties varying as the strain is increased [12]. One of the first studies to investigate the effect of strain rate on the interlaminar fracture toughness of composites was undertaken by Aliyu and Daniel [13]. They used the DCB specimen to study the rate-sensitivity of a carbon fiber reinforced epoxy and observed a 28% increase in the critical strain energy release rate, G_{Ic}, over approximately three orders of magnitude of strain rate. In a subsequent paper, Yaniv and Daniel [14] used a modified DCB specimen to achieve higher crack velocities in a carbon fiber reinforced epoxy composite and reported that the value of G_{Ic} increased with crack velocity up to roughly 1 m/s before dropping at higher rates.

A number of workers have investigated the effect of strain rate on the Mode II interlaminar fracture properties of composite materials. Maikuma et al. [15] used the center notch flexure (CNF) specimen to study rates effects in the delamination resistance of carbon fiber reinforced PEEK. They found that the initiation toughness of this composite under impact conditions was approximately 20% lower than that measured quasi-statically. Blackman et al. [16] used an end-loaded split test geometry to study rate effects in the Mode II delamination behavior of both a thermosetting as well as a thermoplastic-matrix composite and Compston [17] used the end notch flexure geometry to study similar properties in a series of glass fiber reinforced vinylester composites. In both cases, no significant effect of rate on G_{IIc} was observed.

Few workers have investigated the Mode III interlaminar fracture properties of composites, partly as a result of difficulties associated in achieving this type of loading. In an early study, Donaldson [10] used the split cantilever beam (SCB) to investigate the Mode III interlaminar fracture properties of a carbon fiber reinforced epoxy. Lee [18] subsequently developed the edge crack torsion (ECT) to characterize Mode III failure in composites. This test is based on a laminate containing a mid-plane delamination subjected to torsion. In the original test, the specimen was supported on three corners and loaded at the fourth corner. Li et al. [19] used the ECT test to study the Mode III fracture properties of a carbon fiber reinforced epoxy laminate and showed that the Mode III

interlaminar fracture toughness of this system was higher than both its Mode I and Mode II values. Ratcliffe [20] used the ECT test to characterize the Mode III interlaminar fracture toughness of a carbon fiber and a glass fiber reinforced epoxy resin. Here it was shown that the measured values of G_{IIIc} increased rapidly with increasing crack length. Li et al. [21] investigated the effect of varying fiber volume fraction of the Mode III interlaminar fracture properties of a glass/epoxy laminate and reported a large increase in Mode III toughness when the fiber volume fraction was lowered. They also showed that the measured values of G_{IIIc} varied significantly with crack length in composites with both low and high fiber volume fractions.

The aim of this study is to characterize the rate sensitivity of the Mode III interlaminar fracture toughness of a thermoplastic-matrix and a thermosetting-matrix composite material. Initial tests will focus on establishing the influence of crack length on the interlaminar fracture properties of the composite. Following this, tests are undertaken over a range of crosshead displacement rates to characterize the rate-sensitivity of the Mode III interlaminar fracture toughness. A finite element analysis is also used to determine the distribution of the Mode III strain energy release rate along the crack front and to investigate the influence of crack length on the crack-tip loading conditions in these specimens.

EXPERIMENTAL PROCEDURE

The edge crack torsion (ECT) specimen geometry shown in Figure 1 was used to characterize the Mode III interlaminar fracture toughness of the composites investigated in this research programme. Two fundamentally different types of composite were considered, a unidirectional glass fiber reinforced polypropylene with a fiber volume fraction of 35% (Plytron from Gurit Composite Technologies) and a woven glass/epoxy with a fiber volume fraction of 45% (Stesapreg EP127-C15-45 from Stesalit AG). The stacking sequence adopted in the manufacture of the unidirectional glass/polypropylene was:

$$[90, 0, +45, -45, -45, +45, 0, 90]_s$$

whereas the woven glass/epoxy laminates were based on a stacking sequence of:

$$[90/0, (+45/-45)2, (-45/+45)20/90]_s.$$

During lamination, a layer of folded aluminium foil (0.02 mm thick) was introduced at the laminate mid-thickness to act as a starter defect. Panels with dimensions 200 mm × 240 mm were then manufactured in a picture-frame mould using a hot press according to the manufacturer's recommended processing cycle. The nominal final thicknesses of the glass/PP and the glass/epoxy laminates were 4.7 and 6.5 mm respectively. After manufacture, specimens with length Lo and width b dimensions of 108 and 38 mm respectively were removed from the laminates. In Figure 1, it should be noted that the distance L between the points where displacement is applied, is equal to 76 mm. Moreover, each loading pin is located at a distance of 3 mm from the edge of the specimen,

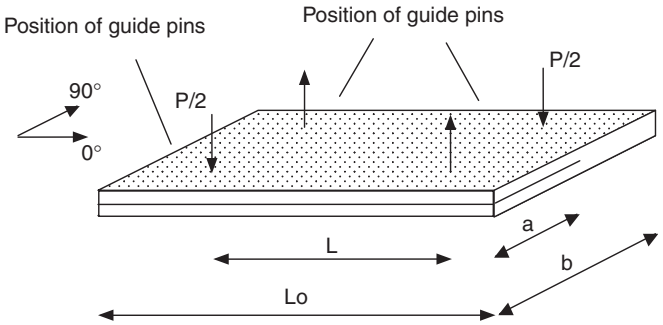

Figure 1. *Schematic of the ECT test specimen.*

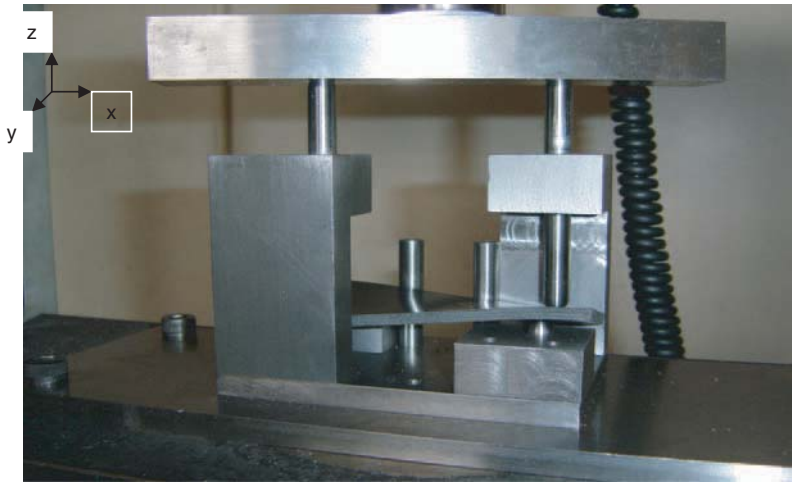

Figure 2. *ECT test fixture.*

in the y direction. Six different normalized initial crack lengths a/b were considered, these being 0.2, 0.3, 0.4, 0.5, 0.6 and 0.7.

The test fixture used for loading the ECT specimens is shown in Figure 2. Here, ECT specimens were placed on two supports positioned at diagonally opposite corners of the test specimen and loaded by two pins located at the two remaining corners. The vertical movement of the two loading pins was ensured by cylindrical holes machined in the test-frame. Three guide pins were positioned on the fixture to enable precise specimen alignment. Two of them were located at the long side of the specimen at a distance of 40 mm from each edge, in the x-axis direction. The third guide pin is located at the middle of the short side of the ECT specimen as shown in Figure 1. The specimen was loaded by applying a force to a horizontal loading bar placed on top of the two loading pins. Initial tests on both types of material system were conducted at a crosshead displacement rate of 2 mm/min on an Instron 4505 universal test machine. Here, the specimens were placed on the ECT test fixture, ensuring that contact was made with all three of the guide pins for precise alignment. After leveling the specimens, load was applied under displacement control. Data acquisition

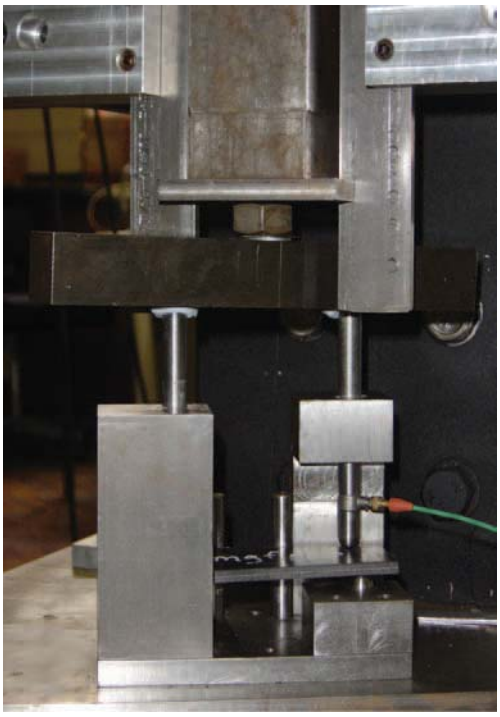

Figure 3. *The modified ECT test fixture for impact testing.*

was assured using a dedicated computer connected to the test machine. Initially, the effect of varying crack length on G_{IIIc} was investigated by testing specimens with different normalized crack lengths, a/b, as discussed above.

The rate-sensitivity of the Mode III interlaminar fracture properties was initially investigated by conducting tests at crosshead displacement rates of 0.2, 2, 20, and 200 mm/min on the Instron 4505 test machine. A limited number of impact tests were also undertaken on the ECT specimens using an instrumented drop-weight impact tower. In these tests, a piezo-electric load-cell was located in one of the two vertical loading pins as shown in Figure 3. The horizontal loading bar was attached to the falling carriage to impact upon the two loading pins as shown in Figure 3. The total mass of the falling carriage including the horizontal loading bar was 2 kg Prior to testing, a small amount of viscoelastic material was placed on top of the loading pins to cushion the impact with the horizontal loading bar. During testing, the impactor was released from a height of 440 mm to give an impact velocity of 3 m/s. The voltage from the piezo-electric load-cell was recorded using the Dataflow software package on a dedicated computer. The resulting voltage–time traces were converted to load–time traces using the load-voltage calibration factor for the load cell.

A Cambridge S360 scanning electron microscope was used to examine the Mode III fracture surface morphology. Sections were taken from the center of the test specimens and examined within 2 mm of the starter crack tip. Specimens were coated with a thin layer of gold prior to examination.

The compliance calibration method, similar to that employed elsewhere [20], was used to determine the Mode III interlaminar fracture properties of the composite materials investigated in this study. Initial attention focused on determining the fracture toughness of the composites at a crosshead displacement rate of 2 mm/min. During each test, load-displacement plots were obtained from which the specimen compliance was determined. The inverse of the specimen compliance, $1/C$, was then plotted as a function of the normalized insert length, a/b, and a straight line was then applied to the data according to:

$$\frac{1}{C} = A\left[1 - m\left(\frac{a}{b}\right)\right] \tag{1}$$

where the parameter correspond to the intercept of the graph with the y-axis and m is the slope of the graph.

The non-linear Mode III fracture toughness of each ECT specimen, $G_{\mathrm{IIIc}}^{\mathrm{NL}}$ was calculated from the load at non-linearity in the load-displacement trace, P_{NL}, using [20]:

$$G_{\mathrm{IIIc}}^{\mathrm{NL}} = \frac{mC}{2Lb[1 - m(a/b)]} P_{\mathrm{NL}}^2 \tag{2}$$

where L is the distance between the supports and b is the specimen width as shown in Figure 1.

The Mode III fracture toughness at maximum load, $G_{\mathrm{IIIc}}^{\mathrm{max}}$, was calculated in a similar fashion using the maximum load, P_{max}.

As a result of material limitations, it was not possible to conduct tests on specimens with the full range of crack lengths at each crosshead displacement rate. Instead, the value of m determined at 2 mm/min was used to calculate G_{IIIc} at all crosshead displacement rates. This was considered acceptable since it is generally accepted that the elastic modulus properties of glass fiber reinforced composites are insensitive to strain rate [22].

Finite Element Analysis

Three-dimensional finite element models of the glass/PP and the woven glass/epoxy specimens were constructed using the ANSYS finite element analysis software package (ANSYS Corporation). The elastic properties used to model the glass/PP and woven glass/epoxy are given in Table 1. The element thickness at the delamination front (in the through-thickness direction) was set equal to one ply thickness, Figure 4, to accommodate for the rapid change in strain field. The element length in the y direction was 0.5 mm and the width in the x direction, 1 mm [20]. For purposes of symmetry, the top and bottom plies of the ECT specimen were modeled using a finer mesh with an element size equal to one ply thickness, this being similar to that used in the vicinity of the crack (Figure 4). Contact elements were used along the delamination plane to prevent mesh interpenetration

Table 1. Material Properties used in the finite element analysis.

Glass Fiber/Polypropylene		
$E_1 = 28$ GPa	$E_2 = 3.72$ GPa	$E_3 = 3.72$ GPa
$\nu_{12} = 0.31$	$\nu_{13} = 0.31$	$\nu_{23} = 0.39$
$G_{12} = 0.644$ GPa	$G_{13} = 0.644$ GPa	$G_{23} = 0.622$ GPa
Woven Glass Fiber/Epoxy		
$wE_1 = 25$ GPa	$E_2 = 25$ GPa	$E_3 = 1.75$ GPa
$\nu_{12} = 0.3$	$\nu_{13} = 0.3$	$\nu_{23} = 0.38$
$G_{12} = 3.5$ GPa	$G_{13} = 3.5$ GPa	$G_{23} = 3.25$ GPa

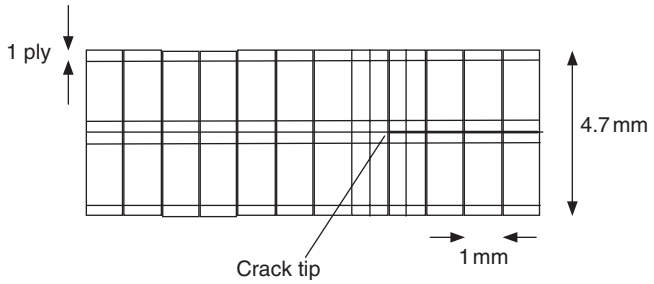

Figure 4. *Finite element mesh of the crack-tip region along the edge of the ECT specimen. Glass/epoxy specimen.*

during the analysis. Relative sliding between points within the delamination region was assumed to be frictionless. The nodes positioned at the location of the guide pins were constrained from moving in the horizontal axes, thereby maintaining contact between the specimen and the pins throughout the analysis. The support pins were modeled by constraining the contact nodes in the vertical, z-axis. For most analyses, a prescribed vertical displacement of 2 mm was applied to the upper surface nodes positioned at the load pins and a geometrically non-linear solution was used in order to update the deformed geometry during the solution process. The reaction loads at the nodes to which displacements were prescribed were calculated and the specimen compliance was determined by dividing the prescribed displacement by the applied load.

The virtual-crack-closure-technique (VCCT) was used to calculate the Mode I, Mode II, and Mode III strain energy release rate components along the delamination front for each of the models examined [23]. The VCCT procedure uses the forces along the crack front and the relative displacements of the crack faces behind the crack tip to determine the three components of the strain energy release rate (G_{I}, G_{II} and G_{III}) [23]. The strain energy release rate components can be calculated from the work required to close the crack to its original length. By summing all of the individual strain energy release rate components, the total strain energy release rate at any location along the delamination front was determined.

$$G_{\mathrm{T}} = G_{\mathrm{I}} + G_{\mathrm{II}} + G_{\mathrm{III}} \tag{3}$$

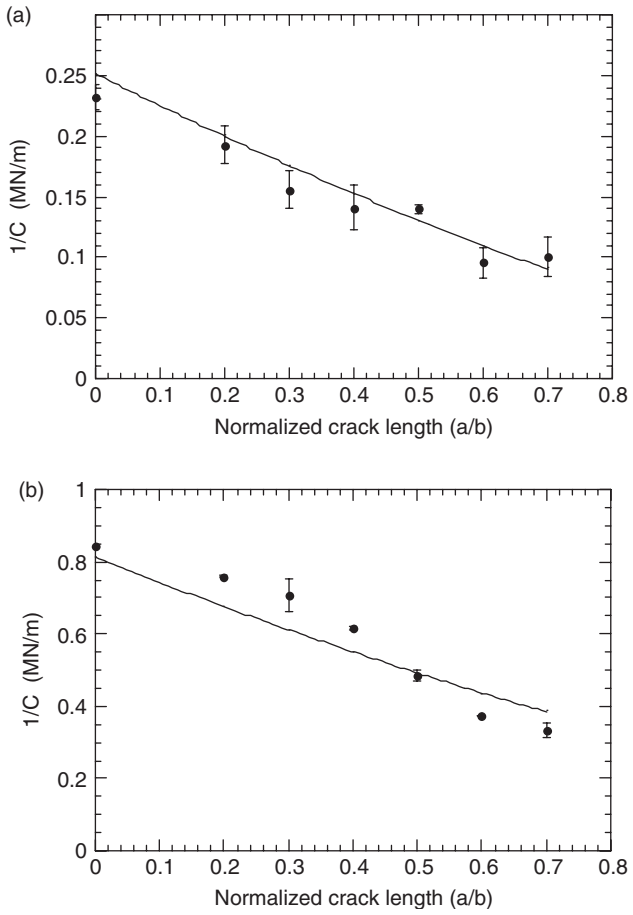

Figure 5. *(a) The variation of the inverse of specimen compliance with normalized crack length for the glass/PP composite. (b)The variation of the inverse of specimen compliance with normalized crack length for the woven glass/epoxy composite.*

RESULTS AND DISCUSSION

Finite Element Model Verification

Initial finite element analyses were undertaken in order to ensure that the finite element solution had fully converged. Here, the size of the elements at the crack tip was decreased from 0.5 to 0.1 mm. The values of G_{II} and G_{III} were virtually identical in all cases, suggesting that the model had converged. In addition, the predictions were compared with those offered by a fine focusing mesh and identical results were obtained. This indicated that the finite element results had fully converged and the predictions of the models were reliable. The accuracy of the finite element model was evaluated by comparing the predicted elastic responses of the ECT specimens with those determined experimentally during the ECT tests. Figure 5(a) shows the variation of the inverse of specimen

compliance (effectively stiffness) with normalized insert length, a/b, for the glass/PP composite specimens. The points in the figures correspond to the experimental data and the solid lines represent the predictions offered by the finite element analysis. Included on the y-axis of the figure are data points corresponding to the elastic response of uncracked plates with the same dimensions as those of the ECT specimen. From the figures, it is evident that the FE predictions are in reasonably good agreement with the experimental data over the range of crack lengths investigated. Closer inspection of the figure indicates that the trends in the experimental data are not completely linear with the gradient tending to reduce with increasing values of a/b. The predictions of the FE analysis also indicated that the plot of the stiffness with crack length was slightly non-linear at the highest normalized crack lengths, supporting the observations from the experimental data. Figure 5(b) shows the corresponding plot for the glass/epoxy specimen where it is again evident that the data do not lie on a straight line as might be expected from Equation (1). Here, the analysis models the elastic response less accurately for the two extremes of crack length with errors of up to 15% being recorded for values of a/b of 0.2 and 0.7. It is likely that these differences are associated with different fiber volume fractions in some of the laminates. A number of panels suffered resin bleed during processing, an effect that will clearly lead to a lower volume fraction of fibers in the resulting laminate. Once again the predictions of the FE analyses suggested that the plot of $1/C$ vs. a/b was slightly non-linear with the slope decreasing slightly at higher crack lengths. In spite of the small degree of non-linearity in the stiffness, Equation (1) was applied to the both the experimental and numerical data to yield the associated values of m.

Strain Energy Release Rate Distribution

Figure 6 shows the variation of G_{III} along the delamination front for both types of composite investigated in this study. Here, the Mode III strain energy release rate is plotted for normalized insert lengths between 0.2 and 0.7. Both figures show similar trends with the value of G_{III} increasing rapidly at the edges before reaching a maximum value closer to the center of the specimen. An examination of the plots indicates that G_{III} is roughly constant over the central region of the test specimen in specimens with intermediate crack lengths whereas two maxima are observed in specimens with shorter and longer insert lengths. The evidence suggests that normalized crack lengths between 0.4 and 0.6 yield relatively flat G_{III} profiles across the central region of the test specimen, representing the most suitable crack configurations when undertaking tests on these materials. A comparison of the two sets of traces in Figure 6 indicates that the calculated vales of G_{III} are higher in the woven glass/epoxy, reflecting the greater rigidity of these laminates. It is also interesting to note that the region over which the value of G_{III} is relatively constant is similar in both sets of materials.

Figure 7 shows plots of the variation of G_{II} along the delamination front for the glass/PP composite. For clarity, only two pre-crack lengths ($a/b = 0.3$ and 0.7) are shown here. The Mode II component, G_{II}, was found to peak at positions corresponding to the location of the load and support pins. This observation has been reported previously by Ratcliffe [20] who argued that, due to the load and support pins, a moment arm is produced which causes relative sliding of the two delaminated sections of the specimen, parallel to the direction in which the delamination tends to grow. From the plots of G_{II}, it can be seen that, as anticipated, the values of the Mode II strain energy release rate are

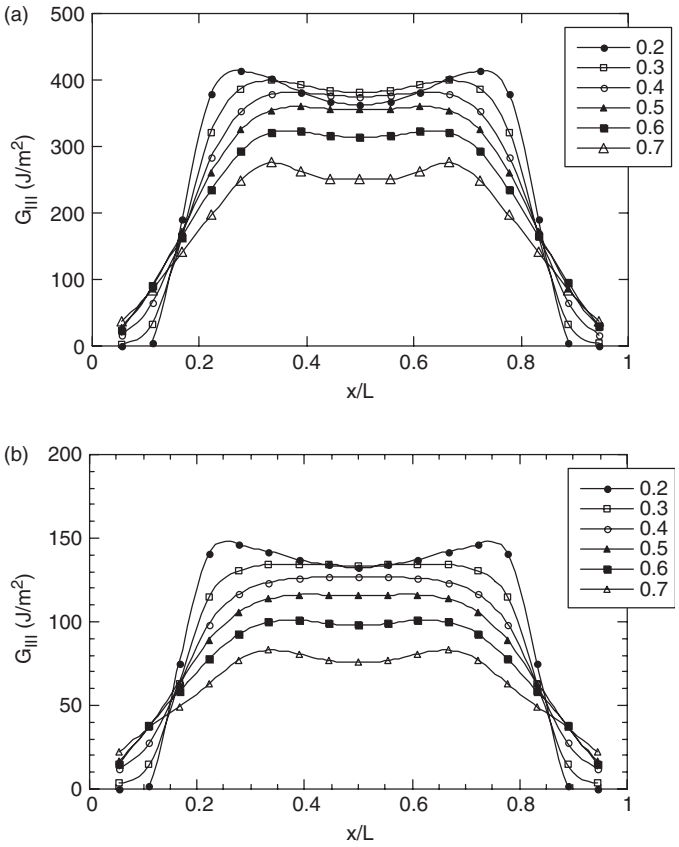

Figure 6. *(a) Mode III strain energy distribution for the glass/epoxy composite as a function of position along the crack front. The numbers of the legend correspond to the normalized crack length a/b. (b) Mode III strain energy distribution for the glass/PP composite as a function of position along the crack front. The numbers of the legend correspond to the normalized crack length a/b.*

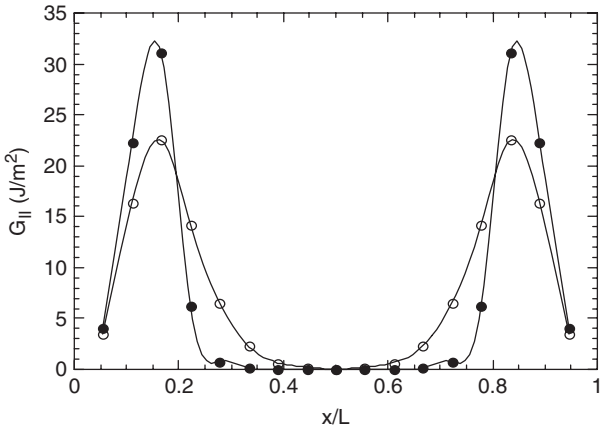

Figure 7. *The distribution of the Mode II strain energy distribution rate across the delamination front in the glass/PP composite. Closed circles a/b = 0.3; Open circles a/b = 0.7.*

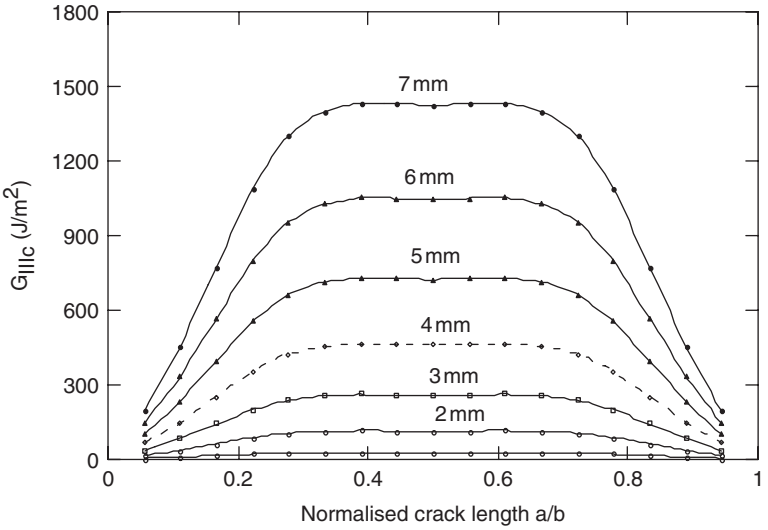

Figure 8. *The distribution of the Mode III strain energy distribution rate across the delamination front in the glass/PP composite for increasing applied displacement. The lowermost curve corresponds to an applied displacement of 1 mm.*

significantly smaller than the corresponding Mode III values. The Mode I component of the strain energy release rate was found to be negligible relative to the value of G_{III} for all the specimens considered in this study and was therefore ignored. Given the relatively small contribution of Mode II loading in these specimens, it is assumed that the ECT test essentially generates a pure Mode III loading condition.

Figure 8 contains a plot of the Mode III strain energy release rate vs. distance along the delamination front for cases where the applied displacement is increased from 1 to 7 mm. These models were conducted on glass/PP ECT specimens with a normalized crack length of 0.5, to determine if the strain energy release rate profiles varied with increasing specimen displacement. As expected, the maximum value of G_{III} increases significantly with the applied displacement, however, the results indicate that the width of the region over which the value of G_{III} is roughly uniform remains the same for all initial displacements and should not, therefore, change during testing.

The effect of varying the thickness of the ECT specimens on the profile of the Mode III strain energy release rate was investigated by increasing the number of grouped +/−45 plies in the glass/PP specimens. Here, finite element models with stacking sequences of $[90/0(+45/-45)_n/(-45/+45)_n0/90]_s$ where $n = 1$, 2, and 3 were constructed and analyzed. In each analysis, the normalized insert length in these 16, 24, and 32 ply laminates was maintained at 0.5 and a prescribed displacement of 2 mm was applied. Figure 9 presents a plots of the variation of the Mode III strain energy release rates along the delamination front for these laminates. As expected, the absolute values of G_{III} increase as the number of plies increases. However, the curves show that the region over which the value of G_{III} is constant is the same in all three specimens, suggesting that, from the point of view of the G_{III} profile, there is no perceived benefit from increasing the thicknesses of the +/−45 plies.

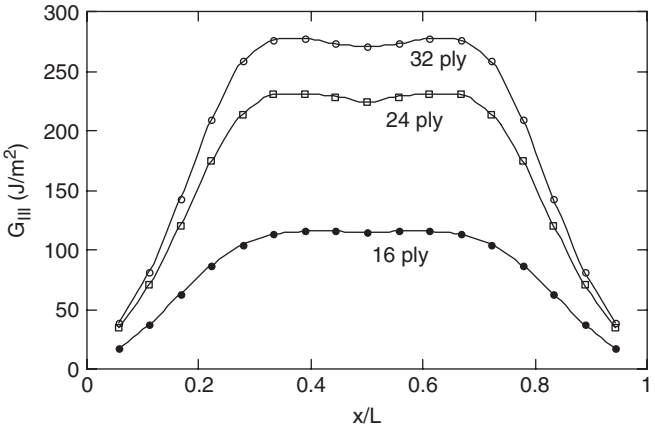

Figure 9. *The distribution of G_{III} across the delamination front for glass/PP laminates with a stacking sequence of $[90, 0(+45, -45)_n/(-45, +45)_n 0, 90]_s$ where $n = 1$ (16 ply), 2 (24 ply) and 3 (32 ply laminate).*

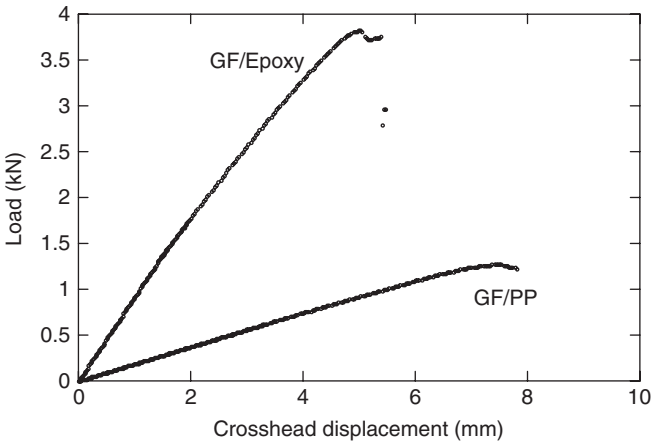

Figure 10. *Typical load–displacement traces following an ECT test on the woven glass/epoxy and the glass/PP composites.*

EXPERIMENTAL RESULTS

Figure 10 shows typical load–displacement traces following ECT tests on both the epoxy and PP-based specimens with a normalized crack length of 0.2. In both specimens, the load increases in a relatively linear fashion, becoming non-linear and reaching a maximum before dropping sharply after macroscopic crack propagation. The Mode III fracture toughness of each ECT specimen was calculated based on the non-linear, P^{NL}, and the maximum load, P^{max} values using Equation (2). The variation of G_{IIIC}^{NL} and G_{IIIc}^{Pmax} are shown as a function of the normalized insert length, a/b, in Figure 11. An examination of the data for the glass/epoxy, Figure 11(a), indicates that the Mode III fracture toughness values increase rapidly with normalized insert length, an effect that has been observed

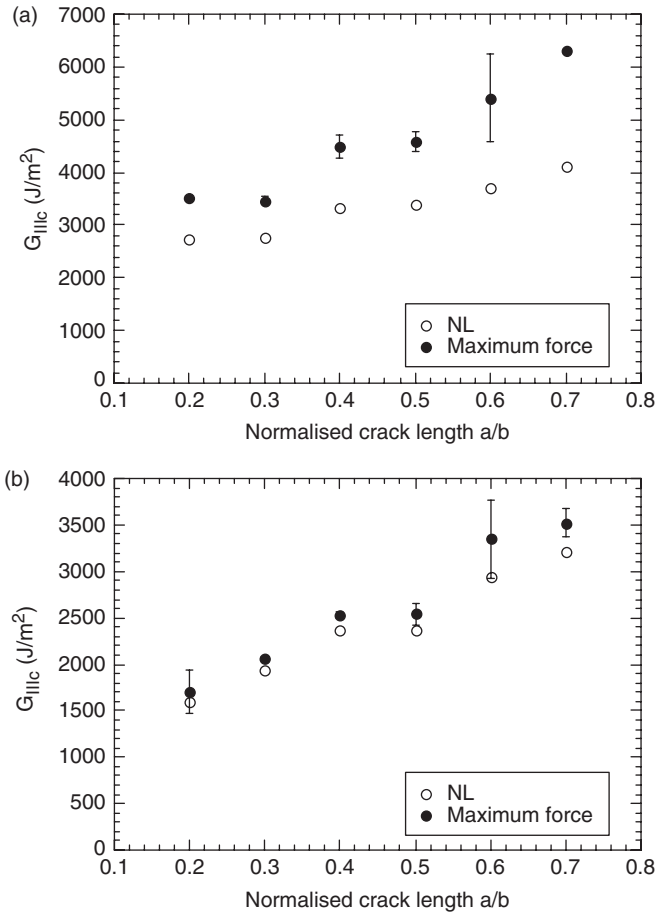

Figure 11. *(a) The variation of G_{IIIc} with normalized crack length for the glass/epoxy laminates. (b) The variation of G_{IIIc} with normalized crack length for the glass/PP laminates.*

elsewhere [20]. Indeed, the values of G_{IIIc} at maximum load increase by approximately 85% over the range of crack lengths considered here. Clearly, such a crack length dependency of G_{IIIc} renders it virtually impossible to determine an intrinsic value of the Mode III interlaminar fracture toughness for this material. It is clear that the values of G_{IIIc} at non-linearity also exhibit an increase with a/b, although the increase is 50% in this case. Figure 11(b) shows the corresponding data for the glass fiber reinforced polypropylene composite. Here, both the non-linear and maximum load values increase sharply with a/b, with the average value for a normalized crack length of 0.7 being roughly double that measured on specimens with an a/b of 0.2. In this case, the non-linear and maximum load values of G_{IIIc} are similar, with the former being approximately 10% lower than the latter. It is not clear why such a crack length dependency exists in these samples. Clearly, frictional effects are likely to be greater in samples with longer crack lengths. However, previous work by Zhao and Wang [26] has shown that this effect is very small in ECT samples. It is possible that crack length effects are associated with the relative

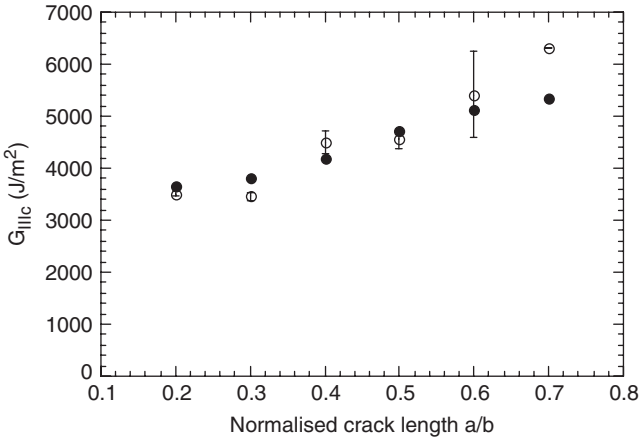

Figure 12. *The Mode III fracture energies of the glass/epoxy calculated using an areas method (open circles). The closed circles correspond to the values in Figure 11(a).*

complex distribution of G_{III} along the crack front, as shown in Figure 6. More research is required to fully investigate this effect.

The crack length dependency of the Mode III interlaminar fracture properties of the composites was further investigated using an areas method to calculate fracture energy. A number of workers have used an areas method to characterize the fracture energy in composites in which crack propagation occurs in an unstable manner [24,25] and this can yield useful information relating to the failure processes. Here, slices were taken at 5 mm intervals in the 90°direction shown in Figure 1. The side of these samples were then ground and the crack length was then measured using an optical microscope. The crack length profiles were then used to estimate the total area of fracture and this was used, along with the area within the load–displacement trace to determine fracture energy. Figure 12 shows the data for the glass fiber reinforced epoxy composite where the data calculated using the areas method are compared with the fracture energies calculated using Equation (2). From the figure, it is clear that the data calculated using the areas method follow a similar trend to the experimental compliance data, increasing rapidly with a/b. This evidence suggests that the crack length dependency of G_{IIIc} is genuine and needs to be considered when conducting Mode III tests of this nature. From the data in Figure 12, it is also clear that the values yielded by the areas method are similar to those calculated using Equation (2).

The influence of crack length on G_{IIIc} was also investigated by conducting a series of finite element analyses in which the displacement at maximum load in the experimental tests, δ_{max}, was used as the imposed displacement in the FE analysis. Here, the VCCT technique was used to determine the maximum value of G_{III} across the crack front for each normalized crack length a/b. Figure 13 presents the predictions of the values of G_{III} at δ_{max} with the experimental data for the glass/PP laminates. It is clear that the maximum values of G_{III} are higher than the values of G_{IIIc} obtained using Equation (2). Clearly, the trends in FE data are similar to those observed experimentally, supporting the observation that the values of Mode III interlaminar fracture energy yielded by the ECT geometry are strongly dependent on initial crack length.

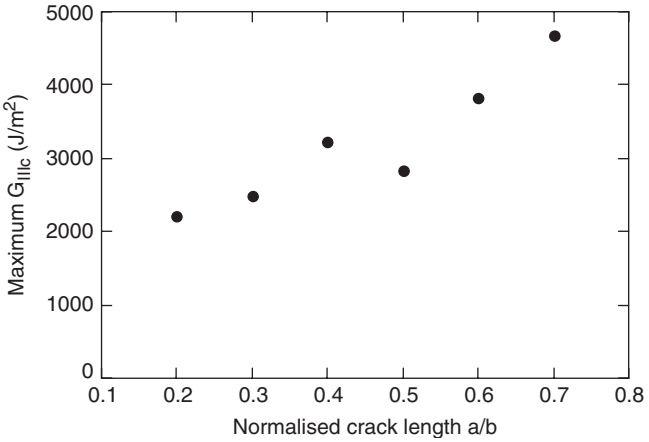

Figure 13. *Predicted values of the maximum values of G_{IIIc} from the finite element analysis as a function of normalized crack length. The displacement at maximum load was used as the imposed displacement in the FE analyses.*

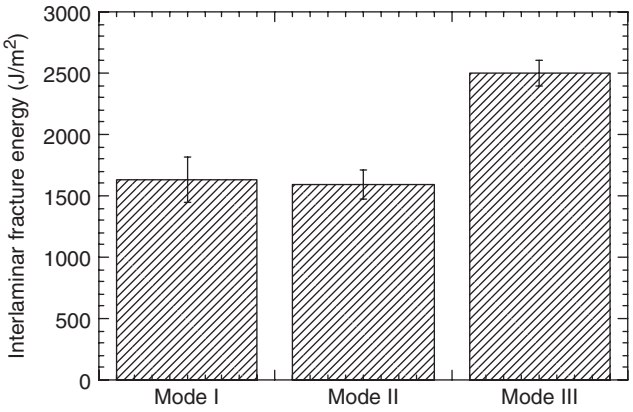

Figure 14. *Interlaminar fracture toughness values for the glass/PP composite. The Mode I and Mode II data are taken from Reference [24].*

Figure 14 compares the Mode III interlaminar fracture properties of the GF/PP composite with that of its Mode I and Mode II values taken from Ref [27]. The cooling rates used to manufacture the panels here were similar to those in Ref [25]. In this figure, the Mode III values for a value of a/b of 0.5 were used. The figure suggests that the Mode III fracture properties are greater than their Mode I and II values. It should be noted however, that the value of G_{IIIc} for a value of a/b of 0.2 is very similar to those values measured under the two other forms of loading, in which case, the interlaminar fracture energy appears to be loading mode insensitive.

The sensitivity of G_{IIIc} to strain rate was initially investigated by conducting tests at crosshead displacement rates between 0.2 and 200 mm/min. The load–displacement traces were similar in all cases to those measured under quasi-static conditions. Figure 15 shows the variation of the measured Mode III fracture toughness for both materials between crosshead displacement rates of 0.2 and 200 mm/min. The normalized crack length, a/b,

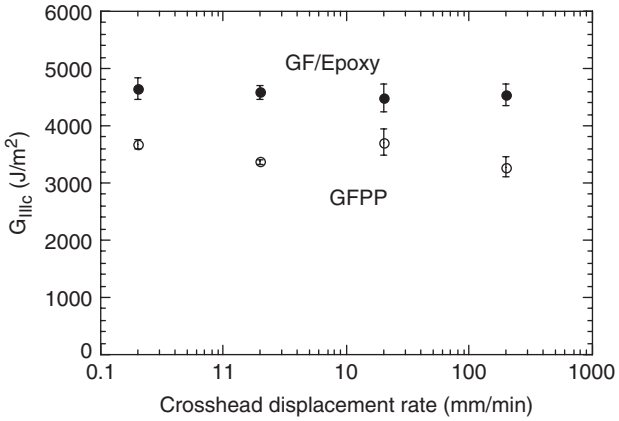

Figure 15. *The influence of crosshead displacement rate on the interlaminar fracture toughness values for the glass/PP and glass/epoxy composites.*

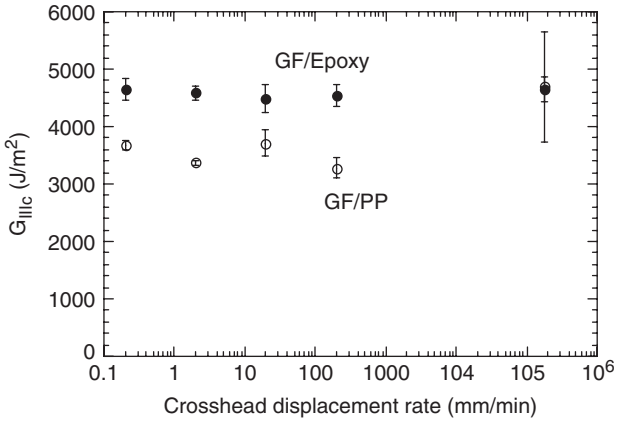

Figure 16. *Comparison of the quasi-static and impact values of interlaminar fracture toughness for the glass/PP and glass/epoxy composites.*

was 0.5 in all cases. An examination of both sets of data indicates that the values of G_{IIIc} remains roughly constant over the range of crosshead displacement rates considered here. Previous work investigating the influence of strain rate on the Mode II fracture properties of this material has also indicated that the interlaminar fracture properties of these composites exhibit very little sensitivity to strain rate [28]. Clearly, the Mode III interlaminar fracture properties of the glass fiber reinforced epoxy remain superior to those of its polypropylene counterpart across the spectrum of crosshead displacement rates, a reflection of the cooling rate dependency of the glass/polypropylene system.

The dynamic fracture properties of the ECT specimens were evaluated through a series of falling weight impact tests on an instrumented drop-weight impact tower. The resulting load–time curves exhibited some initial non-linearity associated with compression of the viscoelastic material placed on the loading pins. Figure 16 compares the rate-dependent response of both material systems where it is clear that the dynamic value of G_{IIIc} for the

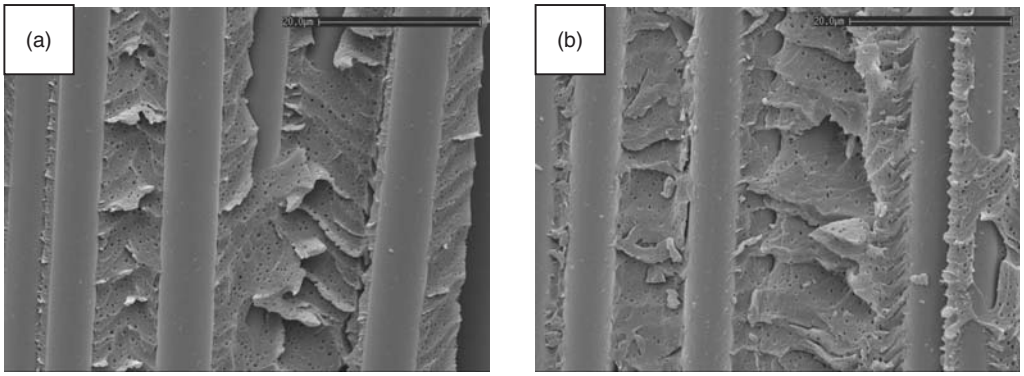

Figure 17. *Electron micrographs of glass/epoxy Mode III specimens tested at (a) 2 mm/min and (b) 3 m/s.*

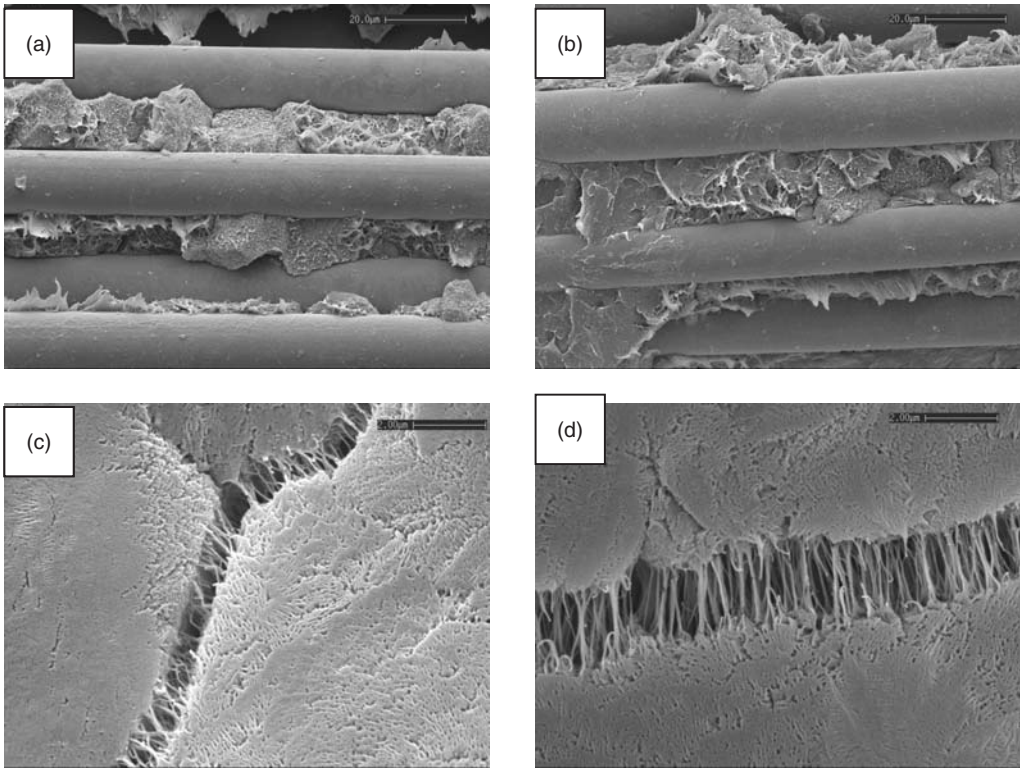

Figure 18. *Electron micrographs of glass/PP Mode III specimens at (a) 2 mm/min, (b) 3 m/s, and (c) 2 mm/min, high magnification, (d) 3 m/s, high magnification.*

epoxy-based specimen is similar to that determined at much lower rates of loading. This evidence suggests that the Mode III interlaminar fracture properties of this system are not sensitive to strain rate. In contrast, the G_{IIIc} values for polypropylene-matrix show an increase at impact rates, suggesting some form of rate-sensitivity.

Fracture surface electron micrographs from specimens tested at the extremes of strain rate studied, 2 mm/min and 3 m/s, are shown for glass/epoxy and glass/PP specimens in Figures 17 and 18, respectively. In each case, the crack growth direction was from left to right and no significant out-of-plane fracture was observed. For the glass/epoxy composite, the 2 mm/min and impacted-loaded specimens in Figure 17(a) and (b) exhibit hackle mark deformation in the matrix. This type of deformation is common for thermoset-based matrices under Mode II loading and is a significant energy absorbing mechanism. Furthermore, in mode II the hackle marks typically lie normal to the fiber direction. Here, under Mode III loading, the hackle marks are oriented at an angle to the fibers; up to 45° in the case of the specimen tested at 2 mm/min. The matrix in the impacted specimen shows slightly less well defined hackle marks and smoother fracture features. This may be an effect of the strain rate. However, the features in both micrographs are similar enough to support the results presented for glass fiber/epoxy in Figure 16, and the conclusion that there is no significant strain rate effect for this composite.

The micrographs for the glass/PP specimens tested at 2 mm/min and low velocity impact are shown Figure 18(a) and (b). Compared to the epoxy matrix, the polypropylene matrix exhibits ductile deformation, which is consistent with observations made for polypropylene-based composite tested under Mode I and II loading. Notably, the deformation features are similar for each specimen despite the difference in strain rate and G_{IIIc} value given in Figure 16. A similarity in deformation features is also observed in the higher magnification micrographs shown in Figure 18(c) and (d). For both strain rates, the cracks between the highly crystalline areas of polypropylene that developed due to the slow cooling during manufacture, are connected by highly deformed strands of polypropylene matrix. It appears, therefore, that the strain rate does not have a significant effect on the Mode III fracture morphology of the glass/PP composite. It is worth noting that many of the fibers in this system were relatively bare suggesting a low degree of fiber–matrix adhesion. The tendency for the crack to propagate along the fiber–matrix interface rather than in the tough polymer may explain the lack of any pronounced rate-sensitivity in the Mode III fracture data.

CONCLUSIONS

A numerical and experimental investigation has been carried out to investigate the Mode III interlaminar fracture properties of a glass/PP and a woven glass/epoxy. A finite element analysis on the ECT specimen has shown that a state of pure Mode III shear exists at the center of the specimen whereas Mode II components exist near the locations of the load and support pins. The experimental evidence indicates that the Mode III interlaminar fracture toughness increases rapidly with increasing insert length rendering it difficult to determine an intrinsic value of G_{IIIc} for these two types of material. The findings of the finite element analysis support these observations with the average values of G_{IIIc}, determined from the measured maximum crosshead displacement, showing a significant increase with normalized crack length.

The effect of varying crosshead displacement rate on the Mode III fracture properties of the two types of composite was studied for a constant value of normalized crack length, a/b. Here, it was shown that the Mode III interlaminar fracture toughness of both systems remained constant at low and intermediate crosshead displacement rates.

Limited testing using an instrumented drop-weight impact tower suggests that the epoxy-based system offers similar fracture properties to those recorded at quasi-static rates of loading. Dynamic tests on the glass/PP system suggest that G_{IIIc} increases at impact rates, although further work is required to substantiate this.

ACKNOWLEDGMENT

The authors are grateful to the EPSRC for financing part of this study.

REFERENCES

1. Schoeppner, G.A. and Abrate, S. (2000). Delamination Threshold Loads for Low Velocity Impact on Composite Laminates, *Composites Part A–Applied Science and Manufacturing*, **31**: 903–915.
2. Prichard, J.C. and Hogg, P.J. (1990). The Role of Impact Damage in Post-Impact Compression Testing, *Composites*, **21**: 503–511.
3. Cantwell, W.J., and Morton, J. (1989). Comparison of the Low and High Velocity Impact Response of CFRP, *Composites*, **20**: 545–551.
4. Dorey, G., Bishop, S.M. and Curtis, P.T. (1985). On the Impact Response of Carbon Fiber Laminates with Epoxy and PEEK Matrices, *Composites Science and Technology*, **23**: 221–237.
5. Dear, J.P. and Brown, S.A. (2003). Impact Damage Processes in Reinforced Polymeric Materials, *Composites Part A -Applied Science and Manufacturing*, **34**: 411–420.
6. Stevanovic, D., Kalyanasundaram, S., Lowe, A. and Jar, P.Y.B. (2003). Mode I and Mode II Delamination Properties of Glass/Vinyl-ester Composite Toughened by Particulate Modified Interlayers, *Composites Science and Technology*, **63**: 1949–1964.
7. Hiley, M.J. (2000). Delamination Between Multi-Directional Ply Interfaces in Carbon-Epoxy Composites Under Static and Fatigue Loading. In: Williams, J.G. and Pavan, A. (Eds), *Fracture of Polymers*, *Composites and Adhesives*, ESIS Publication 27, pp. 61–72.
8. Jordan, W.M., Bradley, W.L. and Moulton, R.J. (1989). Relating Resin Mechanical Properties to Composite Delamination Fracture Toughness, *Journal of Composite Materials*, **23**: 23–943.
9. Pereira, A.B., de Morais, A.B., de Moura, M.F.S.F. and Magalhaes, A.G. (2005). Mode I Interlaminar Fracture of Woven Glass/epoxy Multidirectional Laminates, *Composites Part A -Applied Science and Manufacturing*, **36** (8): 1119–1127.
10. Donaldson, S.L. (1988). Mode III Interlaminar Fracture Characterization of Composite Materials, *Composites Science and Technology*, **32**: 225–249.
11. Meziere, Y., Michel, L. and Carronnier, D. (2000). Mixed-mode Delamination Failure in Carbon Fiber/Composite s Under Quasi-static and Cyclic Loading. In: Williams, J.G. and Pavan, A. (Eds), *Fracture of Polymers*, *Composites and Adhesives*, ESIS Publication 27, pp. 97–110.
12. Grein, C., Kausch, H.H. and Beguelin, P. (2003). The Characterisation of Toughened Polymers by LEFM Using an Experimental Determination of the Plastic Zone Correction, *Polymer Testing*, **22**: 733–746.
13. Aliyu, A.A. and Daniel, I. (1985). In W.S. Johnson (Ed.), *Delamination and Debonding of Materials*, ASTM-STP876, 336.
14. Yaniv, G. and Daniel, I.M. (1988). Height-tapered Double Cantilever Beam for Study of Rate Effects on Fracture Toughness of Composites, *ASTM STP972*, pp. 241–258.
15. Maikuma, H., Gillespie, J.W. and Wilkins, D.J. (1989). Analysis and Experimental Characterization of the Center Notch Flexural Test Under Impact Loading, *J. Composite Materials*, **23**: 757–786.

16. Blackman, B.R.K., Dear, J.P., Kinloch, A.J., MacGillivray, H., Wang, Y., Williams, J.G. and Yayla, P. (1996). The Failure of Fiber Composites and Adhesively Bonded Fiber Composites Under High Rates of Test. Mixed-Mode I/II and Mode II Loadings, *J. Materials Science*, **31**: 4467–4477.
17. Compston, P., Jar, P.-Y.B., Burchill, P.J. and Takahashi, K. (2001). The Effect of Matrix Toughness and Loading Rate on the Mode-II Interlaminar Fracture Toughness of Glass-fiber/Vinyl-ester Composites, *Composites Science and Technology*, **61**: 321–333.
18. Lee, S.M. (1993). An Edge Crack Torsion Method for Mode III Delamination Fracture Testing. *J. Composites Technology and Research*, **15**: 193–201.
19. Li, J., Lee, S.M., Lee, E.W. and O'Bien, T.K. (1977). Evaluation of the Edge Crack Torsion (ECT) Test for Mode III Interlaminar Fracture Toughness of Laminated Composites, *Journal of Composites Technology and Research*, **19**: 174–183.
20. Ratcliffe, J.G. (2004). Characterization of the Edge Crack Torsion (ECT) Test for Mode III Fracture Toughness Measurement of Laminated Composites, NASA/TM-2004–213269.
21. Li, X., Carlsson, L.A. and Davies, P. (2004). Influence of Fiber Volume Fraction on Mode III Interlaminar Fracture Toughness of Glass/epoxy Composites, *Composites Science and Technology*, **64**: 279–1286.
22. Cantwell, W.J. Büsser, M. and Kausch, H.H. (1991). An Analysis of the Impact Response of a Composite Beam, *Composites Engineering*, **1**: 293–307.
23. Shivakumar, K.N., Tan, P.W. and Newman, J.C. (1988). A Virtual Crack Closure Technique for Calculating Stress Intensity Factors for Cracked Three-dimensional Bodies, *International Journal of. Fracture*, **36**: R43–R50.
24. Kalarikkal, S.G., Sankar, B.V. and Ifju, P.G. (2009). Effect of Cryogenic Temperature on the Fracture Toughness of Graphite/epoxy Composites, *Journal of Engineering Materials and Technology*, **128**: 151–157.
25. Yang, Z. and Sun, C.T. (2000). Interlaminar Fracture Toughness of a Graphite/epoxy Multidirectional Composite, *Journal of Engineering Materials and Technology*, **122**: 428–433.
26. Zhao, D. and Wang, Y. (1998). Mode III Fracture Behaviour of Laminated Composites with Edge Crack in Torsion, *Theoretical and Applied Fracture Mechanics*, **29**: 109–123.
27. Davies, P. and Cantwell, W.J. (1994). Fracture of Glass/polypropylene Laminates: Influence of Cooling Rate after Moulding, *Composites*, **25**: 896–877.
28. Cantwell, W.J. unpublished work.